Geomechanics and Engineering, *Vol. 26, No. 6 (2021) 593-605*
https://doi.org/10.12989/gae.2021.26.6.593

Fracture and evolution characteristics of specimens containing double holes

Fanbao Meng[1], Zhijie Wen*[1], Baotang Shen[1,2], Suolin Jing[1], Pubudu Dilan Welgama[1] and Jing Huang[1]

[1]*State Key Laboratory of Mining Disaster Prevention and Control Co-founded by Shandong Province and the Ministry of Science and Technology, Shandong University of Science and Technology, Qingdao 266590, China*
[2]*CSIRO Energy, QCAT, 1 Technology Court, Pullenvale, Qld 4069, Australia*

(Received July 10, 2020, Revised July 9, 2021, Accepted September 27, 2021)

Abstract. Crack initiation, propagation and coalescence, induced by mining stress disturbance are the direct causes of engineering geological hazards which posed a great threat to the safety of coal mining and the stability of engineering rock mass. With the aid of Mining-Induced Stress Test System and Acoustic Emission(AE) monitoring system, the uniaxial compression test of prefabricated large-size double-hole specimens were constructed. The field mining height, the borehole diameter and borehole spacing were reduced in equal proportion. The strength, AE characteristics and fracture evolution process of specimens under different conditions were systematically studied and the dimensionless damage risk coefficient was constructed based on the current research. The formula for the theoretical calculation of reasonable borehole spacing for pressure relief is further revised. Results show that: compared with the complete specimen, the peak strength, elastic modulus and crack initiation stress of the double-hole specimens are significantly decreased. Basically the increase of the hole spacing shows an increasing trend first and then it is decreased. The first tensile crack in the specimen with holes, is initiated close to the hole and it is propagated along the direction of the maximum principal stress. The secondary tensile crack and shear crack are produced with the increase of load and finally the tensile failure mode is formed. An obvious corresponding relationship is shown by the stress curve and AE energy curve. The shear crack always accompanied with a large energy emission rate. The specimens show obvious brittle failure, and internal cracks of the specimens create sudden changes in the rate of AE energy curve and energy accumulation curve. The dimensionless damage risk coefficient can quantitatively characterize the stability of surrounding rock, the revised calculation formula accomplished the field requirements. The research results strengthen the understanding of the mechanism of crack initiation and provide theoretical support for improving the reliability of engineering disaster prediction.

Keywords: crack initiation stress; dimensionless damage risk coefficient; fracture evolution; large-size double-hole specimens; strength characteristics

1. Introduction

The study about stress-strain state and failure mechanism of rock mass is one of the basic topic throughout the development of engineering rock mass mechanics. Initiation, propagation and coalescence of underground cracks are induced due to mining stress disturbance and it directly causes to engineering geological hazards(Sun *et al.* 2019, Kong *et al.* 2019, Erarslan 2016, Leith *et al.* 2014, Gu *et al.* 2020, Baynes 2010, Diederichs *et al.* 2004). Especially with the increase of mining depth and strength year by year, the study on the mechanism of crack propagation and fracture evolution during large-scale rock uniaxial loading has guiding significance for guiding borehole pressure relief in coal mine and selecting reasonable parameters for high slope mining(Wang and Ning *et al.* 2019, Rongkun *et al.* 2017, Meng, *et al.* 2019, Lin *et al.* 2013).

With the application of popularization of fracture mechanics and damage mechanics, many achievements have been made in the strength, deformation characteristics and fracture evolution law of rock with defects(Afolagboye *et al.* 2017, Bahaaddini *et al.* 2013, Tsangouri *et al.* 2019, Huang *et al.* 2017, Li *et al.* 2017, Lin *et al.* 2015, Wang and Tian 2018, Yang *et al.* 2019, Kong *et al.* 2018, Xi *et al.* 2018). For the specimens with prefabricated cracks, in the early 20th century, Inglis(1913) established the model of infinite plate with elliptical hole to show that the concentration of stresses is affected by tensile stress. Shen(1993 and 1995) studied the propagation mechanism of cracks and the rock bridge coalescence process of gypsum specimens with prefabricated cracks under uniaxial compression. Li *et al.* (2009) studied the surface crack propagation model of rock-like materials consisting of cement mortar with special shape. Bobet and Einstein (1998) carried out mechanical tests on gypsum materials with special cracks under different loading modes, crack forms and crack size. Wong (2009a,b) studied the macro and micro mechanisms and laws of crack initiation, propagation and coalescence of gypsum and marble specimens containing prefabricated cracks under uniaxial compression by means of high-speed photography and scanning electron microscopy. Sun and Zhang (2018) studied the AE characteristics of rock materials with

*Corresponding author, Professor
E-mail: sdust0532@gmail.com

ISSN: 2005-307X (Print), 2092-6219 (Online)

prefabricated three-dimensional cracks and crack groups during their propagation under uniaxial compression and multidirectional loading. According to the three-dimensional AE location technology and FRACOD simulation software, the strength, crack propagation law and fracture mechanism of specimens were obtained. For the specimens with prefabricated holes, Zhu and Zhou (Zhou *et al.* 2017, Zhu *et al.* 2015) carried out uniaxial compression tests on small size sandstone specimens with special double voids to study their mechanical properties and evolution mechanism. The numerical simulation and AE technology, of the failure characteristics of specimens with special arrangement of vertical holes were studied for large-sized specimens through laboratory test (Zhao *et al.* 2014). Cai *et al.*(2004) analyzed the generalized crack initiation and crack damage stress thresholds of brittle rock masses near underground excavations. The crack initiation threshold is defined by $\sigma1-\sigma3=A\sigma cm$ and the crack damage threshold is defined by $\sigma1-\sigma3=B\sigma cm$ for jointed rock masses where A and B are material constants and σcm is the uniaxial compressive strength of the rock masses. In order to deepen the understanding of the strength and crack evolution mechanism of existing holes with irregular arrangement, Huang *et al.* studied the strength failure behavior and crack evolution mechanism of granite containing pre-existing non-coplanar holes (Huang *et al.* 2017). Li *et al.* (2020) used digital image correlation (DIC) method to record and analyze the failure behavior of rock, and investigated the fracturing mechanism of rock with combined flaws composed of crack and hole. In order to explore the failure mechanism of rock with holes and fissures, Yang *et al.* (2020 and 2021) carried out a large number of experiments, analyzed the failure behavior and mechanical properties of the samples with composite defects, and studied the evolution results of stress field and crack propagation.

Existing experimental studies on rock mechanics of prefabricated voids and cracks are mainly focused on small-sized specimens with specific void fissures or large width-height ratios and the damage and fracture process of specimens under different combinations of apertures and inclinations (Zhou *et al.* 2017, Han *et al.* 2017, Yang *et al.* 2014). The law of crack initiation, propagation and evaluation of engineering rock massshould be further studied (Wang *et al.* 2020, Jia *et al.* 2020, Zhang *et al.* 2019, Zhang *et al.* 2020). In order to get closer to the site, coal-like samples are made by reasonable material ratio. Reasonable height of coal-like samples is selected to simulate mining height and reasonable borehole diameter is selected to reduce pressure relief hole in coal seam. The influence of different hole spacing on the stability of coal seam is studied by using mining stress test system and AE monitoring equipment. The strength, deformation characteristics, initiation and fracture evolution mechanism of samples are studied in depth and systematically. The dimensionless damage risk coefficient is constructed to quantitatively characterize the stability of the surrounding rock of the stope. It is further extended to provide theoretical and technical support for the selection of borehole parameters for pressure relief in practical engineering and the prediction of stope stability.

2. Introduction of test system and test design

2.1 Introduction to specimens processing

The fractures characteristics and fracture evolution results of rock mass under real load are more discrete due to the complex pore structure of the rock mass and the limitations of current theoretical and experimental methods.In order to meet the requirements of quantitative analysis, by using samples which were designed according to, the Ordinary Concrete Mixture Design Procedures(JGJ55-2011) and the currently available technical literatures (Wang and Wen *et al.* 2018).To carry out the experiment, the mould was first installed and the material mixture was poured into steel mould. Then, the mould was vibrated until the specimens reach enough homogeneity and compactness. The specimens were retrieved from the moulds after 1 day and then cured at room temperature for 30 days. The dimensions of large-size rectangular specimens are 100*100*200 mm for the experiment.To keep the specimen pore structure parameters as consistent as possible, the specimens were made with same mixture ratio, same vibration time interval and the same process parameters.The specimen's faces were carefully polished to maintain the non-parallelism and the non-perpendicularity level to less than 0.02 mm. The specimen's surface is gray and smooth, with no distinct interspace.

The mining height of a coal mine with bursting liability is 8 m, and according to different stress concentration degree, borehole pressure relief was carried out by using 300 mm large aperture row spacing of 1 m, 1.5 m and 2 m, respectively, so as to reduce the regional stress concentration degree and reduce the risk of deformation and failure of surrounding rock of roadway.Simplified specimens were prepared with 200 mm height and 7.5 mm diameter circular holes in equal proportion to 8 m mining height and 300 mm diameter pressure relief hole. The hole spacings (L) were 25 mm, 37.5 mm and 50 mm in specimens with double-hole in single-row. Three specimens were selected from each type. The surface of two vertical circular holes penetrated through the specimens and it was arranged symmetrically along the specimens, as shown in Fig.1. Numbers of 0-1# and 25-1# were used to indicate the Nth test of complete samples with different hole spacing, respectively.

2.2 Loading equipment and method

The mining-induced stress testing machine (Wang and Wen *et al.* 2018) consists of three main parts including the vertical loading system, the lateral loading system and the loading mainframe as shown in Fig.2.The testing system has External Digital Controller(EDC) monitor and Proportion Integral Derivative (PID) control technology (Zhang, and Bar-Ziv 1996).The size of the vertical loading head and vertical load are 150 mm * 100 mm and 900 kN

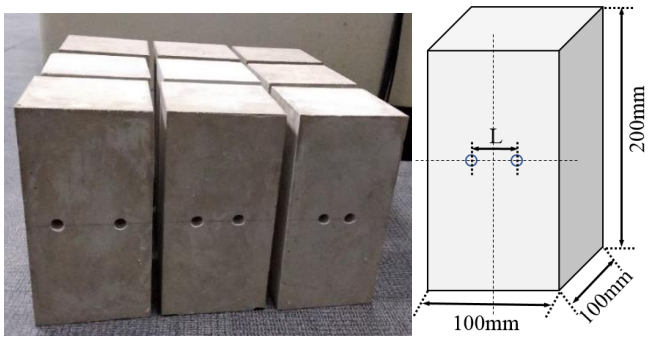

Fig. 1 Double-hole Specimens

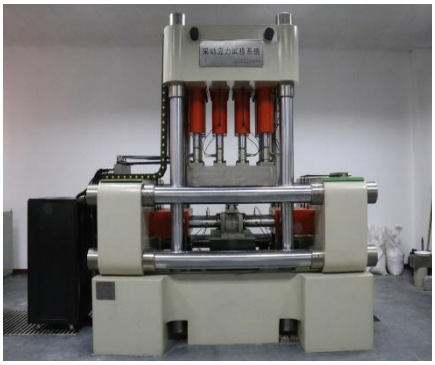

Fig. 2 Mining-induced stress testing machine

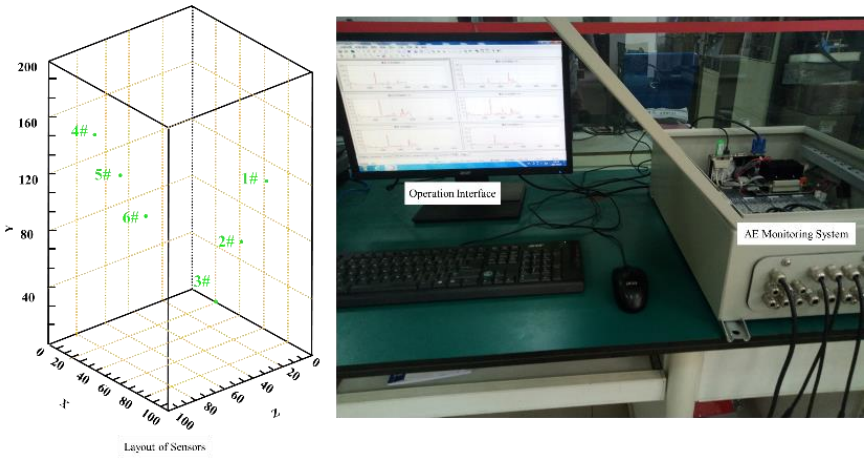

Fig. 3 AE system and sensor distribution

respectively. Ranges of rate of change of, load and displacement are 0.05 kN/s-100 kN/s and 0.05 mm/min-100 mm/min respectively.

Firstly, the vertical load of 0.05 kN was applied as the preset value to ensure the close contact between the testing machine and the specimen. It was also avoided the dynamic impact on the experiment. Then the displacement control method was used to load and select the loading rate of 0.5 mm/min.The jelly couplant Vaseline was used to ensure close contact between the probe and specimen. The specimen was coated with the same type of Vaseline which was used for the sensors, to ensure the accuracy of the experiment and reduce end friction between the loading unit and the specimen during the testing (Wang and Wen *et al.* 2018, Monnier *et al.* 2012, Olsson and, Holcomb 2000). The system can be displayed and record real-time information of mechanical responses of the specimen such as "force-time", "displacement-time" and "stress-strain" graphs to increase the human machine interaction during the experiment. So, it is possible to perform quantitative analysis of the deformation and failure laws of the specimens by using above graphs.

2.3 Data collection system

The phenomenon of strain energy released from rock mass in the form of elastic waves is known as AE. The AE monitoring system of the testing system in Fig.3, is used by the Sensor Highway II (SH-II) monitoring equipment which is developed by Physical Acoustic Corporation (PAC). The

system can be used for stable and accurate real-time monitoring in three-dimensional localization. Three AE sensors of type 3α were arranged on the both surfaces of the specimens in X configuration.AE sensors were fixed to the specimens with tape. The data acquisition system gathers the signals of internal damage of the specimen from AE detectors, which can be used to analyze the rock mass mechanical properties from the macro-meso point of view and it can also provide basic data for subsequent analysis.

Lead breakage test was carried out before starting the test to ensure the amplitude of each sensor signal was above 95 dB. Six channels were used in this test. The AE system and sensor distribution were shown in Fig.3. Threshold values for AE were determined before starting the test. The noise level of the testing machine run at the settled loading rate was not exceed 40 dB, thus, the threshold value of AE system was set to 40 dB. The floating threshold, preamplifier gain, sensor resonance frequency and sampling frequency were set to 6 dB, 40 dB, 20~100 kHz and 10^6 times/s respectively.

In order to reduce the impact of external environment on highly sensitive components of the acoustic emission instrument in the process of the experiment, besides setting the threshold value of acoustic emission signal, we also have taken the relative measures such as minimum number of people in test area, noise-free environment and other into account to conduct the test as accurately as possible. Sony portable digital camera was used to collect real-time images of the whole process of deformation and fracture of specimens under loading.Based on AE signal, stress-strain curve and macro-deformation of the specimen, the mechanical and acoustic emission characteristics of the specimens under uniaxial compression were studied. The strength, deformation characteristics, initiation and fracture evolution mechanism of the specimens with different spacing were analyzed from the point of view of coupling macro-deformation and micro-damage and fracture which can provide basic data for stability analysis of engineering rock mass.

3. Uniaxial compression experiment analysis of double-hole coal-like specimens

3.1 Analysis of mechanical characteristics of specimens

3.1.1 Mechanical Characteristics of Complete Specimens

The stress-strain curves of the complete specimens are shown in Fig.4. The peak front segment of stress-strain curves of the complete specimens basically coincide with each other. The peak stress intensities of specimens are 19.46 MPa, 19.75 MPa and 20.06 MPa respectively. The average peak strength is 19.76 MPa and the standard deviation coefficient is 0.012. The elastic modulus of specimens are 4.72 GPa, 4.60 GPa and 4.77 GPa. The average elastic modulus is 4.697 GPa and the standard deviation coefficient is 0.015. It shows that the homogeneity of specimen material can meet the requirement to have a quantitative data analysis.

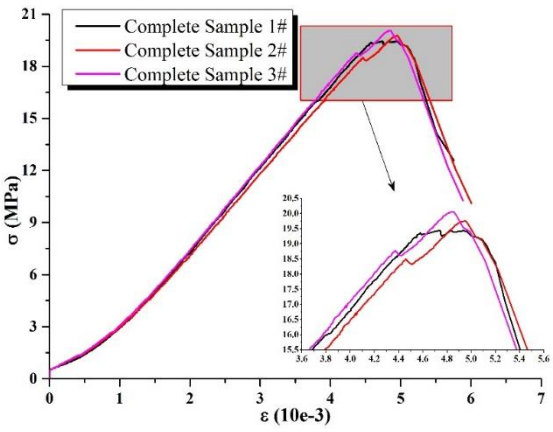

Fig. 4 Stress-strain curves of complete specimens

The stress-strain curves show that the specimens exhibit good linear elasticity characteristics under uniaxial loading. The initial compaction stage changes in arc shape and then enters the elastic stage. When the stress-strain curves approach the peak strength point, the stress drop with different amplitudes. The amplitude drops of specimens 0-2# and 0-3# are 0.12 MPa and 0.16 MPa respectively. Subsequently, the specimen quickly losses its bearing capacity. The stress fluctuation of 0-1# specimen near at the peak strength is clearly different from the stress fluctuation of 0-2# and 0-3# specimens at their failure points. It is considered that the brittleness of 0-1# specimen is relatively weak, and it shows certain transitions from brittleness zone to plasticity zone (Cai *et al.* 2004). Because the performance of 0-1# specimen is obviously different from the remaining two groups, the subsequent data analysis ignores the experimental data. The crack initiation stress is an important index reflecting the structural characteristics of rock defects.

The axial stress of the first macroscopic crack was considered as the crack initiation stress of the specimen in previous studies. The crack initiation stress of the complete specimen was determined as 18.49 MPa according to AE information and video data.

3.1.2 Mechanical properties of specimens with double holes

The most effective samples (25-2#, 37.5-1#, and 50-3# specimens) were selected for the analysis mainly. The stress-strain curves are shown in Fig.5. According to the graphs, peak strength, elastic modulus and crack initiation stress are significantly decreased in double-hole specimens when it is compared with the complete specimens, and initially, above values were increased with the hole spacing increasing and then, those values were decreased. The peak stress and elastic modulus are corresponding to the hole spacing of 37.5 mm. The peak stress and elastic modulus of 25-2#, 37.5-1# and 50-3# specimens are 14.96 MPa, 15.70 MPa and 14.30 MPa respectively. And also, the elastic modulus of 25-2#, 37.5-1# and 50-3# specimens are 4.0071 GPa, 4.1483 GPa and 3.7225 GPa respectively. The peak strength was decreased by 24.3%, 20.5% and 27.6% when it was compared to the average peak strength of complete

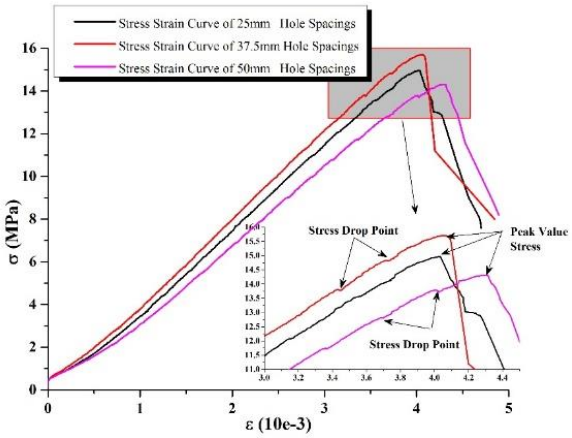

Fig. 5 Stress-strain curves of double-hole specimens with different spacing between holes

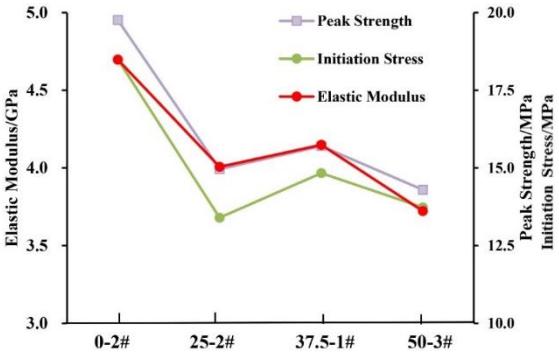

Fig. 6 Characteristic parameter variation diagram of specimens

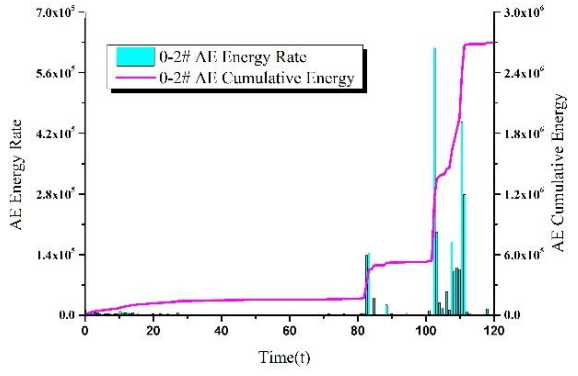

(a) 0-2#

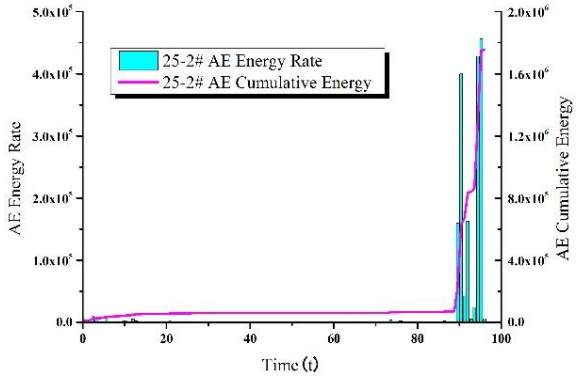

(b) 25-2#

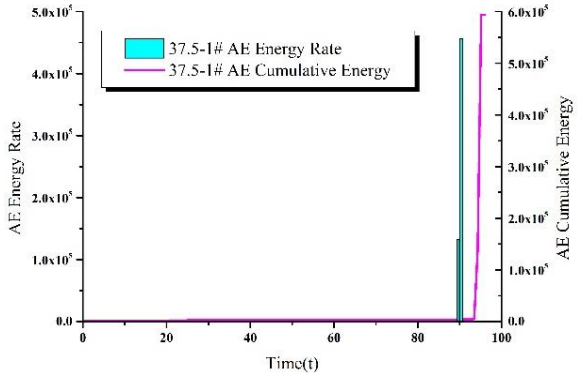

(c) 37.5-1#

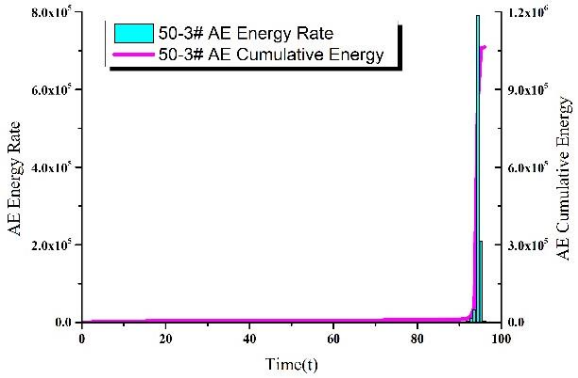

(d) 50-3#

Fig. 7 Schematic diagram of AE energy rate and energy accumulation of double-hole specimens under uniaxial compression.

Table 1 Maximum energy rate and cumulative energy of specimens with different hole spacing

Specimen	Maximum Energy Rate	Cumulative Energy
0-2#	616688	2698160
25-2#	456227	1755099
37.5-1#	455963	594151
50-3#	790248	1063192

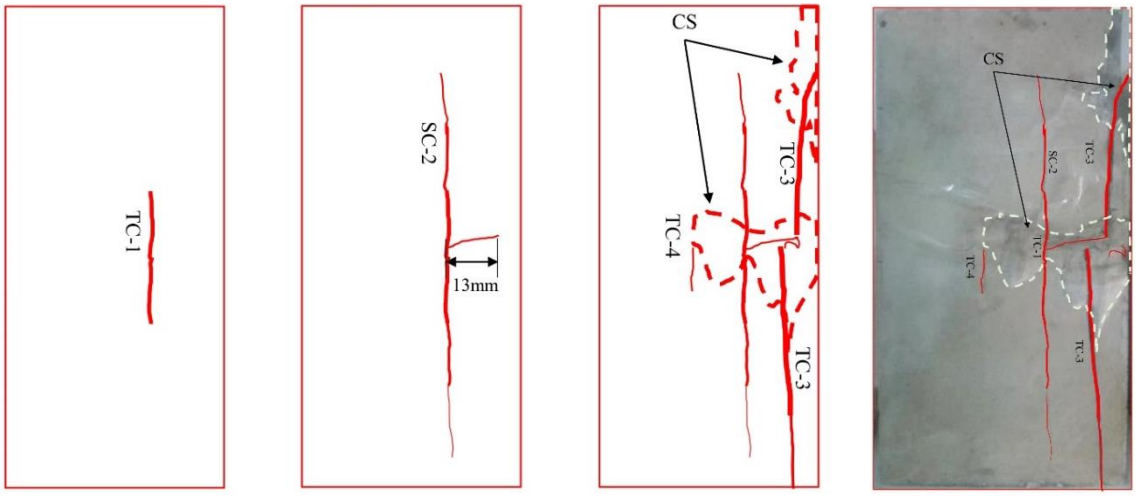

Fig. 8 The fracture evolution process of specimens without hole. In this section, we denote the holes with H-① and H-② respectively; the tensile cracks are indicated by TC; the shear cracks are denoted by SC; the secondary cracks are denoted by Sec; the secondary tensile cracks are denoted by SeTc; The crack is represented by Ec; the range of collapse is indicated by CS

specimens. And also, the elastic modulus was decreased by 14.7%, 11.7% and 20.7% when it was compared to the average elastic modulus of complete specimens. The analysis shows that the stress and influence range of two adjacent holes are superimposed when the distance between two holes are relatively close. So, the two holes can be approximated to a large-scale soft structure. It is easier to produce internal shear failure due to instability under compressive stress, and the bearing capacity is low. The load-bearing capacity, crack propagation resistance and peak strength were correspondingly increased with the increasing of the hole spacing of the specimens. But, above values were gradually decreased when distance between the two holes were further increased. When the hole spacing was further increased, the distance between holes and specimen boundary was reduced so, there was a limitation of increasing hole spacing due to the size of the specimen. When hole spacing further increased, the damage was initiated at the boundary area. The bearing capacity is reduced and the peak strength and elastic modulus are very low then, the two boundaries are failed at the same moment. With the increase of holes spacing, the crack initiation stress of 25-2# 37.5-1# and 50-3# specimens are 13.40 MPa, 14.84 MPa and 13.73 MPa, respectively. As shown in Fig.6, the variation characteristics of the cracking stress are similar to those of the stress peak and the elastic modulus, and crack initiation stress of specimens with two holes are decreased by 19.8% - 27.5%.

3.2 Analysis of AE characteristics

AE Energy Rate and Cumulative Energy curves of specimens with holes under uniaxial compression are shown in Fig.7. Although there is no obvious macro-fracture phenomenon at the initial stage of loading but, still a certain amount of AE energy rate can be detected. Failure of specimens are a cumulative process of damage. A certain level of AE signals can be monitored before obvious macro-cracks are occured and the AE signals are gradually increased with the compression until the AE signals suddenly change and after the energy is released, the AE signals are stabilized. The change of AE signals can be divided into three stages: slow increase in the initial stage, stable in the middle stage and rapid increase in the final stage. At the initial stage of loading (i.e. crack compaction stage), the AE energy values are relatively low, especially for double-hole specimens. With the increase of stress, obvious macro-fracture phenomena are occurred in all the specimens within a certain time range. And only very few energy signals occur in the elastic stage. When the stress is increased continuously, the AE signal is also increased sharply near the damage value of the specimen, and the cumulative curve of AE energy shows a jump mutation, which shows that the specimen begins to produces obvious crack propagation and local collapse, accompanied with larger splitting sound.

The stress curve and AE energy curve of rock specimens show obvious correspondence during loading process.

Large crack propagation in the sample is accompanied with a large AE energy mutation and the initial failure of specimens is often caused by shear cracks. The AE signals of shear cracks are more significant when it is compared to tensile cracks. At the same time, the AE energy rate and cumulative energy of the specimens with holes are initially decreased and then those values are increased with increase of the hole spacing when it is compared with the complete specimens as shown in Table 1. It indicates that the pressure relief of the borehole can be reduced the pressureto a certain extent. The cumulative energy of the specimen and the instantaneous energy release rate, have the lowest values with respective to the hole spacing of 37.5 mm. The pressure relief has a good effect to compare with other scenarios.

3.3 Fracture evolution mechanism of double-hole specimens

3.3.1 Analysis of Fracture Patterns of Complete Specimens

The macro-fracture process of specimens corresponding to the stress-strain curve and the evolution characteristics of AE. There is no obvious macro-fracture phenomenon in the initial stage of compaction under uniaxial loading in 0-2# sample and the stress-strain curve has an arc shape. At the moment, the AE sensor monitors the AE signal with a small energy rate and the initial AE energy rate is gradually decreased with the increase of the axial load. The corresponding cumulative energy is gradually increased and the growth rate is gradually decreased. The cumulative energy curve is in convex shape. Then, the specimen enters to the elastic stage and the stress-strain curve is approximately in a straight line. There is no obvious macro-cracking phenomenon in the elastic stage. The complete specimen produces few energy signals in the elastic stage and the cumulative AE energy curve is approximate to the horizontal. When the axial stressreached to 18.49 MPa, the stress-strain curve shows a stress drop of 0.12 MPa and a tensile crack is occured in the middle of the specimen as shown in Fig.8. The crack is propagated with the increase of stress. and a certain level of AE signals are also produced. The AE energy rate is initially increased and then it is decreased. The maximum AE rate is 143939. With the increase of stress, the shear crack 2 occurs along the middle of the tensile crack 1 at an angle of 15 degrees from the horizontal direction. AE signal was increased sharply with the maximum AE rate of 616688 and the cumulative AE energy curve showed a sudden change which was significantly higher than the AE signal intensity when other cracks were occurred in the existing process. When the shear crack is propagated to 13 mm in length, the stress reaches its peak value of 19.76 MPa. The damage area of the specimen is close to the boundary and the specimen produces obvious longitudinal tensile crack 3 with a failure accompanied by larger splitting sound. At this moment, the AE signal is increased significantly and the maximum AE rate is recorded as 445228. The cumulative curve of AE energy is also increased significantly. The bearing capacity of specimens are decreased drastically and the specimens are damaged.

3.3.2 Analysis of fracture patterns of complete specimens

The fracture evolution process of specimens with hole spacing of 25 mm is shown in Fig.9. At the initial stage of loading, obvious macro-cracking phenomenon was not observed and the AE energy ratio was slightly decreased as it is compared with the complete specimens. Then the AE signal was stabilized and the cumulative curve of AE energy is slightly increased and then remained almost unchanged. When the pressure is close to the initiation stress, the AE energy ratio is started to increase and the cumulative curve of AE energy is also increased. When the axial stress reaches to point a1 of 13.4 MPa, the sample makes splitting sound under the loading of the testing machine. The sample is damaged with shear crack 1 in between the two holes as shown in Fig.9. The AE energy rate is measured as 159844 and the cumulative curve of AE energy is increased linearly. The stress concentration is increased because of the close distance between the two holes. Under the action of compressive stress, the structure is prone to internal penetration instability and it has low bearing capacity. A vertical tensile crack 2 along the principal stress direction is generated in between the two holes at the same time. The crack is continuously developed along the principal stress direction as the stress continues to increase. The monitored maximum AE energy rate in thisprocess is 399887. With the discontinuity of crack growth, the energy accumulation curve rises sharply. As the stress is continuously increased, a small shear crack 3 is developed along the vertical direction of the maximum principal stress at the hole ①. It is propagated in a small range of 1 mm. The maximum AE rate is 162936 and the growth of cumulative energy curve is sharp. Vertical secondary tensile crack 4 was generated at 14.13 MPa at point b1, accompanied by caving and tensile crack 5 and secondary tensile crack 6, which induced the growth of shear crack 7 at the location of hole 2 and monitored in the AE energy rate of 428141. At this time, the internal structure of the whole specimen is in seriously damaged condition and the specimen is also in a very dangerous critical state. If a very small amount of external load is applied to the specimen then, the state of crack development will be changed from stable to unstable state of crack propagation. When the stress is continuously increased to 14.96MPa, the secondary longitudinal tensile crack 8 is propagated along the shear crack 7 at 1 mm away from the hole 2, accompanied with the secondary crack 9, secondary crack 10 and edge crack 11. The strength of the sample is droped sharply, accompanied by its outer surface exfoliation. At this time, the AE signal is increased sharply. The maximum AE energy rate is 456227. The cumulative curve of AE energy shows a sudden fluctuation. The core failure pattern of 25 mm spacing specimen is presented and the failure process is gradually extended from the weak structure inside to the outside. The fracture degree of specimen is high and the crack propagation is complex.

The bearing capacity of 37.5 mm spacing specimen is increased with the increase of spacing. The stress-strain curve of 37.5 mm spacing specimen before peak stress is higher than the 25 mm and 50 mm, spacing specimens. The

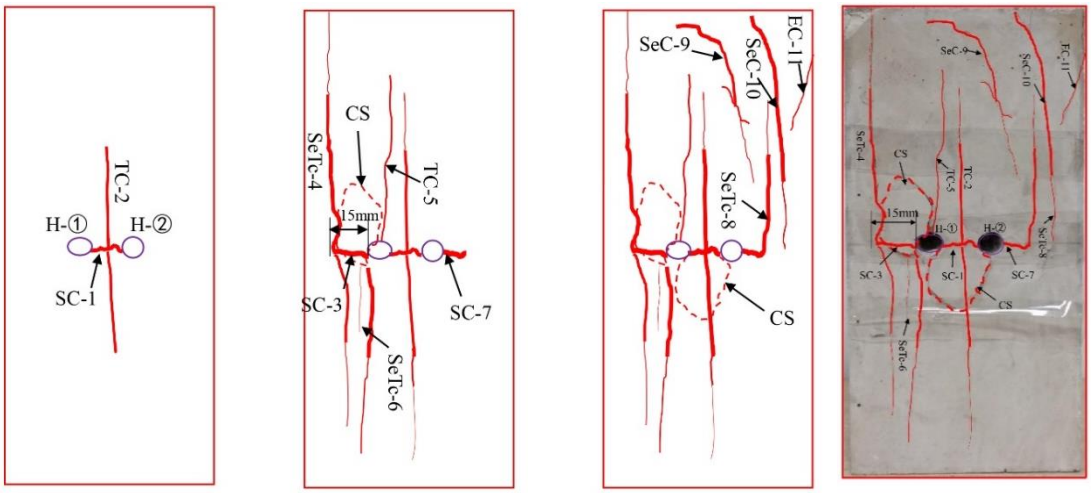

Fig. 9 The fracture evolution process of specimens with 25 mm hole spacing

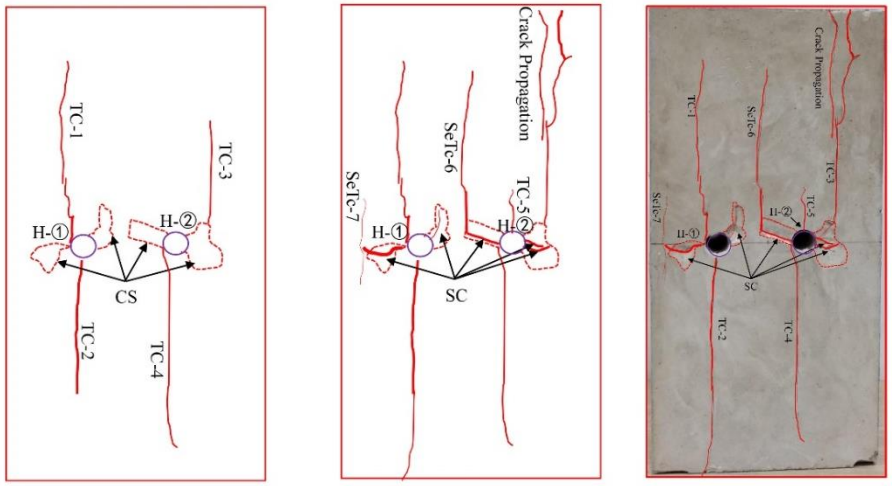

Fig. 10 The fracture evolution process of specimens with 37.5 mm hole spacing

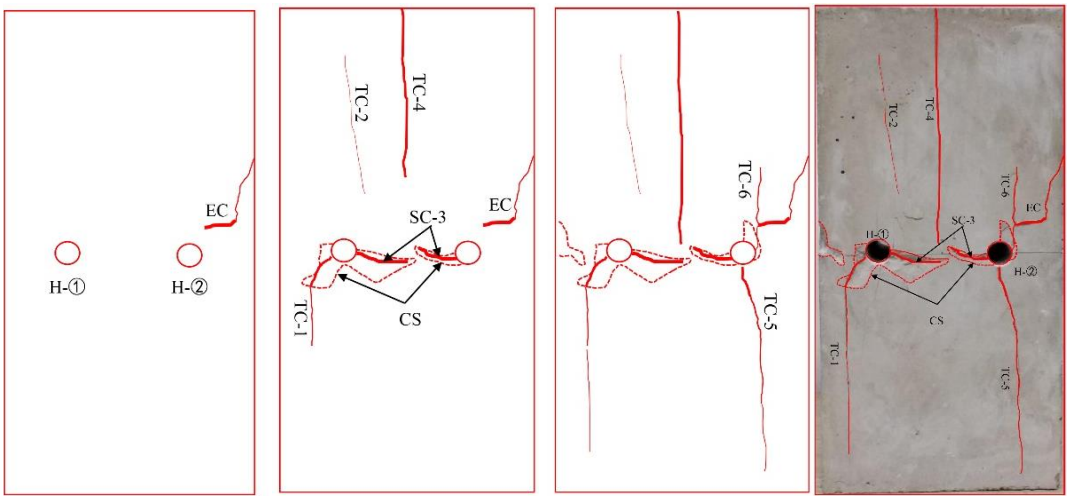

Fig. 11 The fracture evolution process of specimens with 50 mm hole spacing

stress-strain curves and AE characteristics which are obtained from the tests, are relatively simple. At the initial stage of loading, no obvious macro-fracture was observed and the AE energy ratio was again decreased, compared to the 25 mm specimens. As the stress value is gradually increased up to a2 13.80 MPa, the stress of stress-strain curve is dropped by 0.02 MPa, and local collapse occurred close to the two holes. As shown in Fig.10, tensile cracks 4 is propagated along the holes at the same time. When the stress is increased to 14.84 MPa at point b2, the crack is

propagated and the stress-strain curve is again dropped by 0.02MPa. Obvious AE energy signal is not detected during the experiment. When the stress is increased to the peak strength of 15.70MPa at point c2, a larger splitting sound is produced by the specimens and multiple unconnected shear cracks 1 is visible close to the two holes, and they are not connected. With tensile crack 5 and secondary tensile crack 6 and 7, the strength of specimens is dropped sharply but, the AEenergy signal is increased sharply. The maximum AE rate is 455963 and the energy cumulative curve is increased linearly, and the specimens are failed, the experiment is stopped. At this time, the failure of the specimens is independent and the degree of fracture of the specimens is decreased and the number of crack propagation is also decreased.

When the distance between the two holes is further increased the connection between the two holes are gradually weakened. Then, the distance between the two holes and the boundary is also gradually decreased. The damage is initiated at the boundary area where the specimen can be damaged easily. the peak strength is again decreased. There was no obvious macro-cracking phenomenon at the initial stage of the loading process and the energy rate of AE is increased when it is compared with 37.5 mm specimen at the initial stage. As the stress is gradually increased there is a stress drop of 0.02 MPa in 12.82 MPa at point A3, and the edge cracks are propagated above the prefabricated holes ② as shown in Fig.11. As the stress is continued to increase up to 13.78 MPa at point b3, the stress-strain curve is again produced 0.07 MPa stress drop. A wing-shap tensile crack 1 accompany with secondary tensile crack 2, is generated at the hole 1. The shear crack 3 which is not penetrated, is in between the two holes. The tensile crack 4 is rapid and it is initiated from top of the surface to the direction of principal stress at the middle of specimenand the propagation in the direction of principal stress. During this period, the AE signal of the specimen is similar to that of the 37.5 mm hole spacing, and keeps stable until the peak strength of C3 is 14.30 MPa. Tensile crack 5 and wing (tensile) cracks 6 are generated at the hole 2. The strength of the specimen drops sharply, the AE energy signal increases sharply, and the maximum AE rate is 790248. The cumulative energy value rises in a straight line and the experiment stops. The specimen of 50 mm hole spacing has cracks in the direction of outside surface of specimen toward the middle direction. The specimen has minimum strength level, low degree of fracture level and simple crack propagation with few main cracks.

When hole spacing is increased, the failure patterns of specimen is changed from core failure (from internal to boundary failure) to independent failure and then to boundary failure (from external to internal expansion). The actual pressure relief boreholes in coal mines are considered more similar to the 25 mm and 37.5 mm boreholes spacing with few boundary damage.

4. Damage characteristics of rock mass with holes based on crack initiation stress

Based on the study of the fracture evolution mechanism of the above mentioned specimens, it is found that there is a certain relationship between the initiation stress of the specimens and the peak strength of rock mass. In order to apply the research results and field engineering practice, the relationship between cracking stress and peak strength PS/CIS are obtained by analyzing the existing selected specimens. The damage risk factor which is highly influential in stability of field of engineering, is calculated.

Table 2 The relationship between initiation stress and peak strength

	No.	Peak Stress /MPa	Crack Initiation Stress/MPa	PS/CIS
Complete Samples	0-1#	19.46	19.35	-
	0-2#	19.75	18.49	0.936203
	0-3#	20.06	18.64	0.929212
25 mm Hole Spacing	25-1#	15.06	13.98	0.928287
	25-2#	14.96	13.40	0.895722
	25-3#	14.84	13.52	0.911051
37.5 mm Hole Spacing	37.5-1#	15.70	14.84	0.945223
	37.5-2#	10.63	-	-
	37.5-3#	15.86	14.75	0.930013
50 mm Hole Spacing	50-1#	14.19	12.95	0.912615
	50-2#	14.52	13.79	0.949725
	50-3#	14.30	13.73	0.96014

Note: According to the stress-strain curve of 0-1# specimen, the failure pattern is obviously different from other specimens. The different properties of the specimens are not universal due to the preparation process, so it should be omitted in the analysis. Due to low strength of 37.5-2# specimen there is obvious discreteness so, the data analysis is discarded

4.1 Construction of damage risk coefficient

The relationship between initiation stress and peak strength is expressed in dimensionless coordinates. The relationship between initiation stress and peak strength is shown in Table 2. The PS/CIS ratio of specimens is maintained above 0.90 regardless of the hole spacing. Independent from the hole spacing, the stability of specimens can be analyzed and the peak stress of rock mass can be inverted by monitoring the initiation stress of cracks at in situ or indoor conditions.

Based on the above analysis, the dimensionless damage risk factor DRF is defined before the peak point using the Eq. (1).

$$DRF = \frac{\sigma_{CIS}}{\sigma_i} \tag{1}$$

where: σ_i is the stress value at any time; σ_{CIS} is the initial stress value.

When DRF >1, the specimens are in stable state; when DRF=1, damage process of the specimens are started; when DRF reaches 0.9, the specimens are about to fail, so the rock mass should be reinforced in time. The smaller the DRF value is the more serious damage of the surrounding rock mass, until the specimen is failed. DRF index can

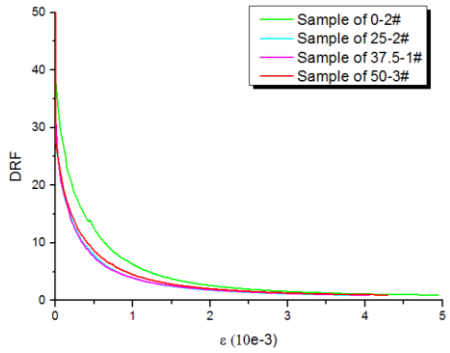

Fig. 12 Non-dimensional damage risk coefficient before peak strength

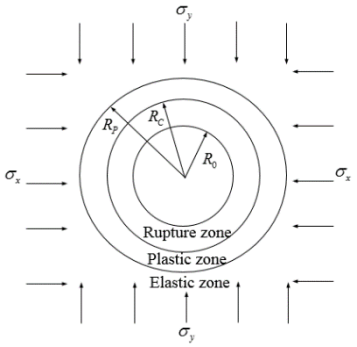

Fig. 13 Stress distribution around boreholes. Where: R_0, R_c, R_p are the radius of borehole, the radius of rupture zone radius and the radius of plastic zone radius, respectively. σ_x is the stress in the horizontal direction; σ_y is the stress in the vertical direction.

reflect the bearing capacity of rock mass in real time and it can quantitatively analyze the stability of in situ at surrounding rock mass.

The stress-strain curves of complete samples and specimens with different hole spacing, are expressed in dimensionless coordinates as shown in Fig.12. The DRF value of rock mass is decreased with time and the stability of rock mass is also decreased accordingly. Based on this, the stability state of rock sample can be clearly characterized and the on-site real-time monitoring which has a guiding role for the stability monitoring of engineering rock mass can be realized.

4.2 Corrected reasonable borehole spacing formula

Large boreholes are formed into rupture zone, plastic zone and elastic zone from inside to outside, as shown in Fig.13 (Lv *et al.* 2019, Han *et al.* 2007). Assuming that the coal body is an ideal elastic-plastic body and adopting the oblique straight-line Coulomb criterion as the failure criterion. Then the radius R_p of the plastic zone can be obtained using the Eq. (2)(Liu 2014 ,Guo *et al.* 2019).

$$R_p = m\omega R_0 \left\{ \frac{\left[\sigma_y(1+\lambda)+2c\cot\varphi\right](1-\sin\varphi)}{2c\cot\varphi} \right\}^{\frac{1-\sin\varphi}{2\sin\varphi}} \left\{ 1+\frac{\sigma_y(1-\lambda)(1-\sin\varphi)\cos 2\theta}{\left[\sigma_y(1+\lambda)+2c\cot\varphi\right]\sin\varphi} \right\} \quad (2)$$

In the formula, m is the correction factor (Considering that there are a lot of random cracks which are not an ideal elastoplastic body, in the coal body. So, the radius of the actual plastic zone is larger). ω is the coefficient of hole enlargement, 1.73-2.44; λ is the coefficient of lateral pressure, 1.1-1.4. R_0 is the radius of borehole, σ_y is the vertical stress, c is the cohesion of coal, φ is the friction angle of coal and θ is the circumferential angle.

The formula of plastic zone is directly calculated by vertical stress. In practical engineering, the mechanical properties of rocks have large differences even under the same stress level at different locations. The formula is further modified using the Eq. (3) by the dimensionless damage risk factor DRF value.

$$R_p = m\omega R_0 \left\{ \frac{\left[\sigma_y(1+\lambda)+2c\cot\varphi\right](1-\sin\varphi)}{2c\cot\varphi} \right\}^{\frac{1-\sin\varphi}{2\sin\varphi}} \left\{ 1+\frac{\sigma_y(1-\lambda)(1-\sin\varphi)\cos 2\theta}{\left[\sigma_y(1+\lambda)+2c\cot\varphi\right]\sin\varphi} \right\} \quad (3)$$

The mining depth of 3310 working face of a coal mine in Shandong Province is 1080 m-1125 m. The impact tendency of three coal samples are tested from the West Wing working face of the coal mine which has strong impact coal seam. Large borehole pressure relief technology is used to relieve pressure and reduce danger. The diameter of borehole, the distance between boreholes and the depth of borehole are 110 mm, 3 m and 15-20 m respectivily.

The crack initiation stress σ_{CIS} is 8.1MPa, the drilling radius R_0 is 0.11 m, the lateral pressure coefficient λ is 1.25, the expansion coefficient ω is 2, the correction coefficient of coal plastic zone m is 2.5, coal cohesion c is 1.1 MPa, friction angle in coal body φ is 30° and circumferential angle θ is 45°.

By substituting the parameters into the modified plastic zone formula, the influence radius $R_p^{'}$ is selected as 0.9 m in a single pressure relief borehole. So, the acceptable distance is 2 m in between the pressure relief boreholes. The effect of pressure relief is further tested in sequence with on-site microseismic monitoring. The microseismic results show that the seismic activity is decreased. When the microseismic activity energy level is below 10^4 J, the risk of rock burst is low.

5. Discussion

Based on the above results, it is found that the load-carrying capacity of specimens is related to the dominant crack form. The load-carrying capacity of specimens with main tensile form fracture (such as complete specimens, 37.5 mm hole spacing) is higher than the specimens with significant shear form fracture (such as 25 mm, 50 mm). When the specimen reaches the initial cracking stress value, the specimen goes to unsafe state. The specimen is destabilized and destroyed by applying very small amount of stress. Based on this, the dimensionless damage risk factor which can reflect the real time bearing condition is proposed for rock mass. Thus, this can be used for the quantitative analysis of rock mass stability in engineering.

It is also found that with the increase of the distance between the two holes, the failure patterns of the specimen changed from the core failure to the boundary failure, that is, from the internal damage transfer to the boundary to the

external crack expansion to the internal. The actual pressure relief boreholes in coal mines are more similar to borehole spacing of 25 mm and 37.5 mm there are few boundary cracks (borehole spacing 50 mm). The elastic modulus, peak strength and initial cracking stress of specimens are, initially increased and then decreased. The working mechanism of pressure relief drilling, the stress-strain results and AE characteristics of the test are analyzed together. The optimum pressure relief effect is based on the lowest energy stored in the specimen and the lowest energy release rate, while ensuring the specimen still has a certain strength. The results show that an optimal hole spacing is existed when distance between two holes is increased.

When the research results are compared with the previous studies on small-size specimens, it shows that the size of specimens has a strong relationship on the failure characteristics of specimens. Whatever compression mode is adopted for small-size specimens, when the specimens is ultimately ruptured, the rock bridge will generally run through and the cracks are generally inclined distribution, accompanied by obvious shear cracks. Tensile cracks are also penetrated the whole process of crack evolution for large size specimens. The shear cracks can be characterized the load-bearing capacity of the specimen to a certain extent. When the development of shear crack is increased, the load-bearing capacity goes down. In the process of specimen size becoming smaller to larger, the failure process of specimen changes from shear failure of small size to splitting failure of large size gradually.

The existing theoretical formulas for calculating reasonable borehole spacing are directly calculated by vertical stress. The mechanical properties of rocks at different locations have significant differences under the same stress level in practical engineering . In this paper, the formula is further modified by the dimensionless damage risk factor DRF value. The dimensionless damage risk coefficient is constructed and the formula for the theoretical calculation of reasonable borehole spacing for pressure relief is further revised, based on the current research. The dimensionless damage risk coefficient can be quantitatively characterized the stability of surrounding rock in stope, and the calculation results of the modified theoretical calculation formula of reasonable pressure relief borehole spacing meet the requirements of field construction.

There are many coupling factors in underground rock mass engineering. So, the process of rock mass crack, propagation and development should be further researched. In this paper, existing research simplifies the working face and the different spacing of single row holes are only studied systematically. However, the actual pressure relief method adopted in the working face should also be taken into account in different situations such as the spatial distribution of different drilling holes. The influence of the weakening space formed by different pore combinations on the stability of samples will be systematically studied in the following articles.To a certain extent,theoretical guidance can be provided by the research results for pressure relief drilling and rock burst prevention in working face.

With the aid of Mining-Induced Stress Test System and Acoustic Emission(AE) monitoring system, the uniaxial compression test of prefabricated large-size double-hole specimens were constructed. This study had limitations, and further studies are needed. Only uniaxial compression tests were performed, and only the effect of the space of hole on mechanical behavior was investigated in this study. In future studies, the influences of the geometry of the holes (for example, the number and the layout of holes) and other stress conditions on the mechanical properties and cracking behavior should be assessed.

It has been shown that the spatial distribution of AE events can reflect the law of crack initiation and propagation. Before the failure of rock specimens, the spatial distribution of AE events implies the trend of macroscopic crack propagation and predicts the final location of macroscopic cracks. In the loading process of this test rock specimens, the same positioning method and the same sensor layout are adopted, but no representative AE positioning results are obtained. Some studies think that the main reason for not getting the positioning results is that the rock specimens with good homogeneity have fast propagation speed, so no effective AE events were detected. Some scholars believe that at the moment of destruction, the acoustic emission signal waveform is continuous, so it can not form a positioning event. Although there is no effective AE location event, it does not affect the research of fracture patterns, AE characteristics and mechanical properties of specialties with double holes. In the future, the test method will be optimized to obtain the AE location event when the specimen is damaged, and the relationship between AE event spatial location and crack initiation is analyzed in detail.

6. Conclusions

Compared with the complete specimens', the peak strength, elastic modulus and crack initiation stress with the double-hole specimens, all parameters are decreased significantly, and basically with the increase of the hole spacing showed a trend of increased first and then decreased.

The stress curve and AE energy curve are shown obvious corresponding relationship during the loading process. The shear crack always accompanies with AE energy rate. It is also found that with the increase of the distance between the two holes, the failure patterns of the specimen changes from core failure (from internal to boundary failure) to independent failure and finally to boundary failure (from external to internal expansion).

When the specimen reaches the initial cracking stress value, the specimen goes to dangerous state and the specimen will be destabilized state. It is failed by applying a very small amount of stress after above states. Based on this, the dimensionless damage risk factor of rock mass which can reflect the bearing condition of rock mass in real time and realize the quantitative analysis of rock mass stability in engineering, is proposed. The smaller the DRF value is, the more serious the surrounding rock damage will be until the specimen is failed.

The best pressure relief effect should be based on the

lowest energy stored in the specimen and the lowest energy release rate, while guaranteeing that the specimen is still having a certain strength. The results show that the optimal hole spacing exists with the increase of the distance between two holes.

The research results strengthen the understanding of the mechanism of crack initiation and development in engineering rock mass and provide theoretical support for improving the reliability of engineering disaster prediction.

Acknowledgments

This study was supported by Shandong Provincial Natural Science Foundation of China (ZR2019BEE013), National Natural Science Foundation of China (No. 51974174 and 51974173), the Shandong Provincial Excellent Youth Scientists Fund (grant No. ZR2019YQ26). The authors are grateful to the reviewer for his/her valuable comments and suggestions.

Conflict of interest

The authors declare that they have no conflict of interest.

References

Afolagboye, L.O., He, J., and Wang, S. (2017), "Experimental study on cracking behaviour of moulded gypsum containing two non-parallel overlapping flaws under uniaxial compression", *Acta Mech. Sinica*, **33**(2), 394-405. https://doi.org/10.1007/s10409-016-0624-9.

Bobet A. and Einstein H.H. (1998), "Numerical modeling of fracture coalescence in a model rock materials", *Int. J. Fracture*, **92**(3), 221-252. https://doi.org/10.1023/A:1007460316400.

Bahaaddini, M., Sharrock, G. and Hebblewhite, B.K. (2013), "Numerical investigation of the effect of joint geometrical parameters on the mechanical properties of a non-persistent jointed rock mass under uniaxial compression", *Comput. Geotech.*, **49**, 206-225. https://doi.org/10.1016/j.compgeo.2012.10.012.

Baynes, F.J. (2010), "Sources of geotechnical risk", *Q. J. Eng. Geol. Hydroge.*, **43**(3), 321-331. https://doi.org/10.1144/1470-9236/08-003.

Cai, M., Kaiser, P.K., Tasaka, Y., Maejima, T., Morioka, H. and Minami, M. (2004), "Generalized crack initiation and crack damage stress thresholds of brittle rock masses near underground excavations", *Int. J. Rock Mech. Min. Sci.*, **41**(5), 833-847. https://doi.org/10.1016/j.ijrmms.2004.02.001.

Diederichs, M.S., Kaiser, P.K, and Eberhardt, E. (2004), "Damage initiation and propagation in hard rock during tunnelling and the influence of near-face stress rotation", *Int. J. Rock Mech. Min. Sci.*, **41**(5), 785-812. https://doi.org/10.1016/j.ijrmms.2004.02.003.

Erarslan, N. (2016), "Microstructural investigation of subcritical crack propagation and Fracture Process Zone (FPZ) by the reduction of rock fracture toughness under cyclic loading", *Eng. Geol.*, **208**, 181-190. https://doi.org/10.1016/j.enggeo.2016.04.035.

Gu H.L., Tao M., Li X.B., Cao W.Z. and Li Q.Y. (2020), "Dynamic response and meso-deterioration mechanism of water-saturated sandstone under different porosities", *Measurement*, **167**,1-12. https://doi.org/10.1016/j.measurement.2020.108275.

Guo, X.F., Zhao, Z.Q., Gao, X., Xu, X.Y. and Ma, N.J. (2019), "Analytical solutions for characteristic radii of circular roadway surrounding rock plastic zone and their application", *Int. J. Min. Sci. Technol.*, **29**(2), 263-272. https://doi.org/10.1016/j.ijmst.2018.10.002.

Han, C.R., Bai, S.W., and Zhang, B. (2007), "Analysis of stress distribution near borehole in orthotropic rockmass with stress calculus of variations", *Rock Soil Mech.*, **28**(12), 2593-2597. https://doi.org/10.1007/s11747-006-0011-3.

Han, G.S., Jing, H.W, Su, H.J, Zhu, T.T., Du, M.R., Xiong, F. and Wu, J.Y. (2017), "Experimental study on compressive strength and fracture characteristics of sandstone containing double circular cavities", *J. China Coal Soc.*, **42**(4), 871-878. https://doi.org/10.13225/j.cnki.jccs.2016.0792.

Huang, Y. H., Yang, S.Q., Ranjith, P.G. and Zhao, J. (2017), "Strength failure behavior and crack evolution mechanism of granite containing pre-existing non-coplanar holes: Experimental study and particle flow modeling", *Comput. Geotech.*, **88**,182-198. https://doi.org/10.1016/j.compgeo.2017.03.015.

Inglis, C.E. (1913), "Stresses in a plate due to the presence of cracks and sharp corners". *Inst. Naval Architect. London*, **55**, 219-230.

Jia, C.Y., Wang, H.L., Sun, X.Z., Yu, X.B. and Luan, H.J. (2020), "Study on rockburst prevention technology of isolated working face with thick-hard roof", *Geomech. Eng.*, **20**(5), 447-459. https://doi.org/10.12989/gae.2020.20.5.447.

Kong, R., Feng, X.T, Zhang, X.W, and Yang, C.X. (2018), "Study on crack initiation and damage stress in sandstone under true triaxial compression", *Int. J. Rock Mech. Min. Sci.*, **106**, 117-123. https://doi.org/10.1016/j.ijrmms.2018.04.019.

Kong, P., Jiang, L.S., Shu, J.M., Sainoki, A. and Wang, Q.B. (2019), "Effect of fracture heterogeneity on rock mass stability in a highly heterogeneous underground roadway", *Rock Mech. Rock Eng.*, **52**(2), 1-18. https://doi.org/10.1007/s00603-019-01887-5.

Leith, K., Moore, J.R., Amann, F., and Loew, S. (2014), "In situ stress control on microcrack generation and macroscopic extensional fracture in exhuming bedrock", *J. Geophys. Res.*, **119**(1), 594-615. https://doi.org/10.1002/2012JB009801.

Li, D.Y., Zhu, Q.Q., Zhou, Z.L., Li, X.B. and Ranjith, P.G. (2017), "Fracture analysis of marble specimens with a hole under uniaxial compression by digital image correlation", *Eng. Fract. Mech.*, **183**, 109-124. https://doi.org/10.1016/j.engfracmech.2017.05.035.

Li, D.Y., Gao, F.H., Han, Z.Y. and Zhu, Q.Q. (2020), "Full- and local-field strain evolution and fracture behavior of precracked granite under coupled static and dynamic loads", *Shock Vib.*, (8), 1-15. https://doi.org/10.1155/2020/8866673.

Li, M.T., Li, S.C., Yang. L. and Zhang, N. (2009), "Experimental study of the surface crack propagation mode in rock-like materials", *J. Exp. Mech.*, **24**(1), 21-26. https://doi.org/10.1360/972009-754.

Lin, P., Wong, R.H., and Tang, C.A. (2015), "Experimental study of coalescence mechanisms and failure under uniaxial compression of granite containing multiple holes", *Int. J. Rock Mech. Min. Sci.*, **77**, 313-327. https://doi.org/10.1016/j.ijrmms.2015.04.017.

Lin, P., Zhou, Y.N., Liu, H.Y. and Wang, C. (2013), "Reinforcement design and stability analysis for large-span tailrace bifurcated tunnels with irregular geometry", *Tunn. Undergr. Sp. Technol.*, **38**(9),189-204. https://doi.org/10.1016/j.tust.2013.07.011.

Liu, S.H. (2014), "The study on the mechanism and prevention of

dynamic-loading rockburs", Ph.D. Dissertation, Coal Science Research Institute, Beijing, China.

Lv, A., Masoumi, H., Walsh, S.D., and Roshan, H. (2019), "Elastic-softening-plasticity around a borehole: An analytical and experimental study", *Rock Mech. Rock Eng.*, **52**(4), 1149-1164. https://doi.org/10.1007/s00603-018-1650-7.

Meng, F.B, Wen, Z.J., Shen, B.T., Jiang, Y.J., Shi, S.S. and Zhao, R.L. (2019), "A pplicability of yielding–resisting sand column and three-dimensional coordination support in stopes", *Materials*, **12**(16), 2635.
https://doi.org/10.3390/ma12162635.

Monnier, T., Seydou, D., Godin, N. and Zhang, F. (2012), "Primary calibration of acoustic emission sensors by the method of reciprocity, theoretical and experimental considerations", *J. Acoust. Emission*, 152-166.
https://doi.org/10.1016/0042-207X(66)90610-5.

Olsson, W.A. and Holcomb, D.J. (2000), "Compaction localization in porous rock", *Geophys. Res. Lett.*, **27**(21), 3537-3540.
https://doi.org/10.1029/2000GL011723.

Rongkun, P., Fu, D., Yu, M.G. and Lei, C. (2017), "Directivity effect of unloading bedding coal induced fracture evolution and its application", *Int. J. Min. Sci. Technol.*, **27**(5), 825-829.
https://doi.org/CNKI:SUN:ZHKD.0.2017-05-016.

Shen, B.T. (1993), "Mechanics of fractures and intervening bridges in hard rocks", Ph.D. Dissertation, Royal Institute of Technology, Stockholm, Sweden.

Shen, B.T, Stephansson, O., Einstein, H.H., and Ghahreman, B. (1995), "Coalescence of fractures under shear stresses in experiments", *J. Geophys. Res.*, **100**(6), 5975-5990.
https://doi.org/10.1029/95JB00040.

Sun, W.B., Du, H.Q., Zhou, F. and Shao, J.L. (2019), "Experimental study of crack propagation of rock-like specimens containing conjugate fractures", *Geomech. Eng.*, **17**(4), 323-331.https://doi.org/10.12989/gae.2019.17.4.323.

Sun, X.Z, Zhang B.L., Yin, D.W. and Shen, B.T. (2018), "Experimental study of three-dimensional cracks propagation characteristics under uniaxial compression", *J. Basic Sci. Eng.*, **27**(04), 890-905.
https://doi.org/10.16058/j.issn.1005-0930.2019.04.017.

Tsangouri, E., Remy, O., Boulpaep, F., Verbruggen, S., Livitsanos, G. and Aggelis, D.G. (2019), "Structural health assessment of prefabricated concrete elements using acoustic emission: Towards an optimized damage sensing tool", *Constr. Build. Mater.*, **206**, 261-269.
https://doi.org/10.1016/j.conbuildmat.2019.02.035.

Wang, C.X., Shen, B.T., Chen, J.T., Tong, W.X., Jiang, Z., Liu, Y. and Li, Y.Y. (2020), "Compression characteristics of filling gangue and simulation of mining with gangue backfilling: An experimental investigation", *Geomech. Eng.*, **20**(6), 485-495.
https://doi.org//10.12989/gae.2020.20.6.485.

Wang, J., Ning, J.G., Jiang, L., Jiang, L.S. and Bu, T. (2018), "Structural characteristics of strata overlying of a fully mechanized longwall face: A case study", *J. S. Afr. I. Min. Metall.*, **118**(11),1195-1204.
https://doi.org/10.17159/2411-9717/2018/v118n11a10.

Wang, X. and Tian L.G. (2018), "Mechanical and crack evolution characteristics of coal-rock under different fracture-hole conditions: A numerical study based on particle flow code", *Environ. Earth. Sci.*, **77**(8), 1-10.
https://doi.org/10.1007/s12665-018-7486-3.

Wang, X., Wen, Z.J., Jiang, Y.J. and Huang, H. (2018), "Experimental study on mechanical and acoustic emission characteristics of rock-like material under non-uniformly distributed loads", *Rock Mech. Rock Eng.*, **51**(3), 1-17.
https://doi.org/10.1007/s00603-017-1363-3.

Wong, L.N.Y. and Einstein, H.H. (2009a), "Crack coalescence in molded gypsum and Carrara Marble: Part 1-Macroscopic observations and interpretation", *Rock Mech. Rock Eng.*, **42**(3), 475-511. https://doi.org/10.1007/s00603-008-0002-4.

Wong, L.N.Y. and Einstein, H.H. (2009b), "Crack coalescence in molded gypsum and Carrara Marble: Part 2-Microscopic observations and interpretation", *Rock Mech. Rock Eng.*, **42**(3), 513-545. https://doi.org/10.1007/s00603-008-0003-3.

Xi, X., Yang, S.T. and Li, C.Q. (2018), "A non-uniform corrosion model and meso-scale fracture modelling of concrete", *Cement Concrete Res.*, **108**, 87-102.
https://doi.org/10.1016/j.cemconres.2018.03.009.

Yang, S.Q. and Huang, Y.H. (2014), "Experiment and particle flow simulation on crack coalescence behavior of sandstone specimens containing double holes and a single fissure", *J. Basic Sci. Eng.*, **22**(3), 584-597.
https://doi.org/10.3969/j.issn.1005-0930.2014.03.017.

Yang, S.Q., Yin, P.F., Zhang, Y.C., Chen, M., Zhou, X.P. and Jing, H.W. (2019), "Failure behavior and crack evolution mechanism of a non-persistent jointed rock mass containing a circular hole", *Int. J. Rock Mech. Min. Sci.*, **114**, 101-121.
https://doi.org/10.1016/j.ijrmms.2018.12.017.

Yang, S.Q., Yang, Z., Zhang, P.C. and Tian, W.L. (2020), "Experiment and peridynamic simulation on cracking behavior of red sandstone containing a single non-straight fissure under uniaxial compression - sciencedirect", *Theor Appl Fract Mec* , **108**, 1-19. https://doi.org/ 10.1016/j.tafmec.2020.102637.

Yang, S.Q., Tian, W.L., Liu, X.R., Huang, Y.H. and Yang. J. (2021), "An experimental study on failure mechanical behavior and cracking mechanism of rectangular solid sandstone containing two non-coplanar fissures under conventional triaxial compression", *Theor. Appl. Fract. Mec.*, **114**, 1-17.
https://doi.org/10.1016/j.tafmec.2021.102975.

Zhang, G.L., Ranjith, P.G., Li, D.Y., Wanniarachchi, W.A.M. and Zhang, B.N. (2020), "In situ synchrotron x-ray microtomography observations of fracture network evolution of coal due to waterflooding", *Geophys. Res. Lett.*, **47**(10).
https://doi.org/10.1029/2020GL087375.

Zhang, S.C., Li, Y.Y., Shen, B.T., Sun, X.Z. and Gao, L.Q. (2019), "Effective evaluation of pressure relief drilling for reducing rock bursts and its application in underground coal mines", *Int. J. Rock Mech. Min. Sci.*, **114**, 7-16.
https://doi.org/10.1016/j.ijrmms.2018.12.010.

Zhang, X.F. and Bar-Ziv, E. (1996), "A 3D position controller for a charged particle suspended in a modified electrodynamic chamber", *Rev. Sci. Instrum.*, **67**(10), 3483-3490.
https://doi.org/10.1063/1.1147163.

Zhao, X.D., Zhang, X.H. and Zhu, W.C. (2014), "Fracture evolution around pre-existing cylindrical cavities in brittle rocks under uniaxial compression", *T. Nonferr. Metals Soc.*, **24**(3), 806-815. https://doi.org/10.1016/S1003-6326(14)63129-0.

Zhou, Y., Liu, B., Wang, L., Li, X. and Ding, G.P. (2017), "Mesoscopic mechanical properties of rock-like material containing two circular holes under uniaxial compression", *Chin. J. Rock Mech. Eng.*, **36**(11), 2662-2671.
https://doi.org/10.13722/j.cnki.jrme.2017.0501.

Zhu, T.T, Jing, H.W., Su, H.J., Yin, Q. and Du, M.R. (2015), "Mechanical behavior of sandstone containing double circular avities under uniaxial compression", *Chin. J. Geo. Eng.*, **37**(6), 1047-1056.https://doi.org/10.11779/CJGE201506011.

CC